325

Liquid metal flow in a U-bend in a strong uniform magnetic field

By S. MOLOKOV and L. BÜHLER

Kernforschungszentrum Karlsruhe GmbH, Institut für Angewandte Thermo- und Fluiddynamik, Postfach 3640, 76021 Karlsruhe, Germany

Magnetohydrodynamic flows in a U-bend and in a right-angle bend are considered with reference to the toroidal concepts of self-cooled liquid-metal blankets. The ducts composing the bends have rectangular cross-sections. The applied magnetic field is aligned with the toroidal duct and perpendicular to ducts supplying liquid metal. For high Hartmann numbers the flow region is divided into cores and boundary layers of different types. The magnetohydrodynamic equations are reduced to a system of partial differential equations governing wall electric potentials and the core pressure. The system is solved numerically. The results show that the flow is very sensitive to variations of certain parameters, such as the wall conductance ratio and the aspect ratio of the toroidal duct cross-section. Depending on these parameters, the flow exhibits a variety of qualitatively different flow patterns. In particular, structures of helical and vortex type are obtained. A high-velocity jet occurs at the plasma-facing first wall and there is mixing of the fluid in the toroidal duct. These factors lead to desirable heat-transfer conditions.

1. Introduction

Magnetohydrodynamic (MHD) flows play an important role in liquid-metal cooled fusion reactor blankets. Since an electrically conducting fluid has to flow through regions of the plasma-confining strong magnetic field, currents are induced within the fluid. They close their loops in thin boundary layers and in electrically conducting channel walls and cause a considerable pressure drop and quite a different flow pattern compared to conventional hydrodynamic flows.

In several blanket designs efforts have been made to achieve high velocities for an effective heat transfer in the plasma-facing first-wall coolant channels. Several authors have proposed reducing the MHD pressure drop by aligning the flow direction with the main toroidal component of the magnetic field. Toroidal channels are fed by larger poloidal ones (Smith *et al.* 1985) or by radial channels (Malang *et al.* 1988). In these channels, where the flow suffers from strong MHD interaction, over a short distance the fluid flows perpendicular to the field. Both designs of liquid metal blankets involve MHD flows in straight ducts where the magnetic field is nearly perpendicular to the mean flow direction or nearly hydrodynamic flow in ducts aligned with the magnetic field, provided that the ducts are long enough that fully developed flow is established far away from the junctions between ducts.

The MHD and conventional hydrodynamic flows in straight ducts are radically different. The MHD flow exhibits a core and boundary layers because the ratio of electromagnetic to viscous force given by the square of the Hartmann number, $M = B_0 L(\sigma/\rho\nu)^{\frac{1}{2}}$, is large. Here B_0 is the applied constant magnetic field, L is a characteristic

dimension of the cross-section and σ, ρ, ν are the electrical conductivity, density and kinematic viscosity of the fluid, respectively. In fusion applications M typically varies in the range of 10^3–10^4. In fully developed MHD flows in rectangular ducts two main types of boundary layers occur. The first type, which is called the Hartmann layer, appears at walls perpendicular to magnetic field lines. Its thickness is $O(M^{-1})$. The Hartmann layer matches variables in the core, where viscous effects are negligible, to the boundary conditions at the wall. The flow in the Hartmann layer is governed by a system of ordinary differential equations. If the magnetic field is tangential to a channel wall, referred to as a sidewall by many authors, the second type of boundary layer appears at this wall with the dimensionless thickness $O(M^{-\frac{1}{2}})$. The flow in this layer is governed by a system of convective heat-conduction equations, and therefore this layer is called parabolic. For large values of M this layer can carry an $O(1)$ volume flux, since high fluid velocities, $O(M^{\frac{1}{2}})$, are possible inside. If there is no component of the magnetic field perpendicular to duct walls, i.e. the magnetic field is aligned with the flow, the velocity profile is of Poiseuille type similar to that in fully developed hydrodynamic flows.

   For convenience, we call the ducts with axes perpendicular to the magnetic field the radial ducts, according to the blanket concept presented by Malang et al. (1988), whereas ducts aligned with the field are called the toroidal ducts. However, the discussion and the results are equally applicable to the poloidal–toroidal–poloidal concept (Smith et al. 1985).

   Radial and toroidal ducts are connected by bends which may cause considerable three-dimensional effects on the pressure drop and velocity distribution. The geometry of a symmetric radial–toroidal–radial U-bend, which is typical of a toroidal concept of a liquid-metal blanket, is shown in figure 1(a). The characteristic length L is half the distance between the sidewalls. This geometry includes two limiting cases. One is a 90° bend for $y < l$, if the length of the toroidal duct is infinite ($l \to \infty$); the other is the 180° bend, if the toroidal duct length reaches its smallest value $l = a$. The magnetic field may be perfectly aligned with the toroidal direction $\hat{y}$, as assumed in the present investigation, or slightly turned in the (x, y)-plane by the angle of α; 90° bends with positive or negative inclination α are called forward and backward elbows, respectively.

   Since flow types in radial and toroidal ducts are expected to be radically different, at least in the regions close to the junction at $x = 0$, the flow is essentially three-dimensional. Three-dimensional effects in bends, which are critical issues for any toroidal concept, have been estimated for $\alpha = 0°$ by Hunt & Holroyd (1977), Aitov, Kalyutik & Tananaev (1979) and Hunt (cited by Holroyd 1980), and investigated experimentally by Holroyd (1980) and Barleon et al. (1993b). All theoretical works referred to are based on the assumption that the magnetic field is uniform and not affected by the flow (small magnetic Reynolds number).

   Hunt & Holroyd (1977) and Hunt (cited by Holroyd 1980) present simple order-of-magnitude estimates of the qualitative flow behaviour in a 90° bend for insulating ($c = 0$) or poorly conducting ($c \ll 1$) channel walls. Here, $c = \sigma_w t/\sigma L$ is the wall conductance ratio, σ_w and t are the wall conductivity and the thickness, respectively. On the basis of the theory of characteristic surfaces, Hunt & Holroyd (1977) predict high-velocity jets, which carry nearly the whole volume flux in the region near $z = \pm 1$. If ducts are rectangular, these jets are confined to thin boundary layers of dimensionless thickness $O(M^{-\frac{1}{2}})$ or $O(N^{-\frac{1}{3}})$ if either $N \gg M^{\frac{3}{2}}$ or $N \ll M^{\frac{3}{2}}$, according to Hunt & Leibovich (1967). In the above $N = \sigma L B_0^2/\rho v_0$ is the interaction parameter, which corresponds to the ratio of electromagnetic to inertial forces; v_0 is a characteristic velocity. If $N \gg M^{\frac{3}{2}}$, inertial effects can be neglected (Hunt & Leibovich 1967).
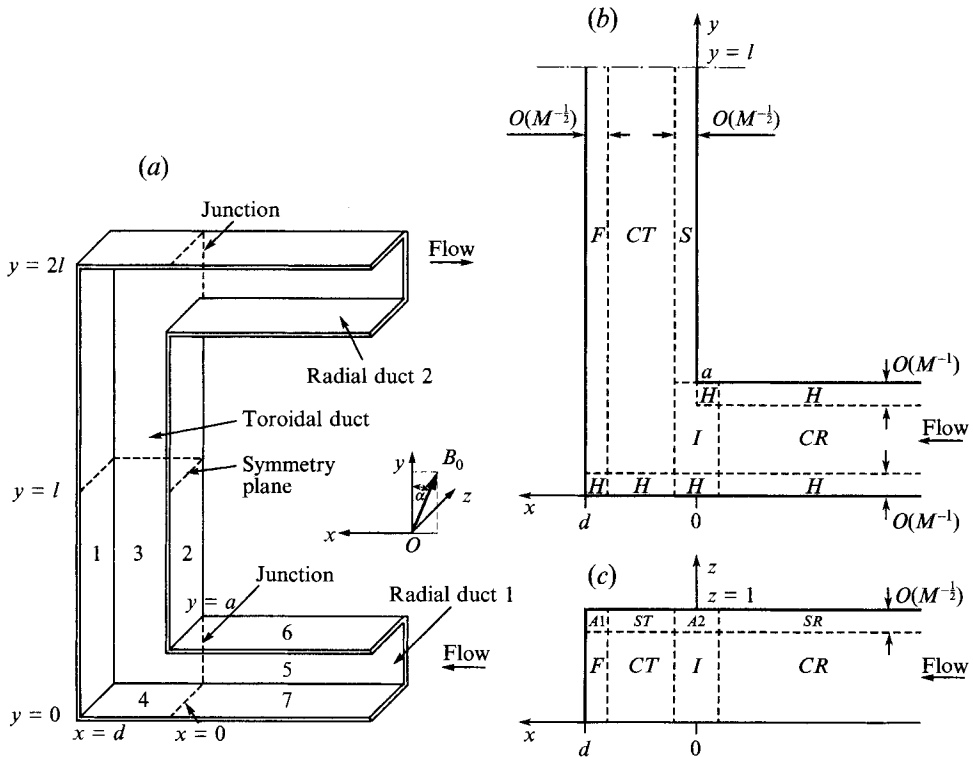
FIGURE 1. (a) The geometry of a U-bend for $z > 0$. Walls are numbered as follows: 1, blanket first wall; 2, second wall; 3, sidewall of the toroidal duct; 4, bottom of the toroidal duct; 5–7, sidewall, top and bottom of the radial duct 1. (b, c) Flow subregions at large Hartmann number: CR, core of the radial duct; CT, core of the toroidal duct; H, Hartmann layers; SR, ST, layers at sidewalls 3 and 5; F and S, layers at the first and second walls; I, internal layer.

Depending on the liquid metal and the duct geometry, the parameter N may vary in the range of 10^2–10^5.

However, a completely different flow pattern might be established, as has been suggested by Hunt (cited by Holroyd 1980). On the basis of order-of-magnitude arguments Hunt predicts the flow confined to a layer of thickness $O(N^{-\frac{1}{3}})$ for $N \ll M^{\frac{3}{2}}$ at $x = 0$. It should be noted that for $N \gg M^{\frac{3}{2}}$ the layer would have the thickness $O(M^{-\frac{1}{2}})$. Since these two flow patterns differ 'radically – perhaps too radically', Holroyd (1980) suggested that 'the true flow is probably more complex and contains features of both models'.

Aitov *et al.* (1979) solved numerically the full set of nonlinear equations governing three-dimensional MHD flows in a U-bend with $\alpha = 0°$ and $c = 0$. This approach allows calculations to be made only for flows at relatively low Hartmann numbers ($M \leqslant 30$) which are not relevant to fusion-blanket applications. The qualitative results presented show the tendency of the fluid to flow at the sidewalls in the region of the bend, in accordance with the prediction by Hunt & Holroyd (1977). Unfortunately, the lack of details in that paper makes a quantitative comparison with the results presented here impossible.

There is a number of theoretical and experimental papers which treat flows in bends with $\alpha \neq 0°$: Moon & Walker (1990), Moon, Hua & Walker (1991), Hua & Walker (1991), Kunugi, Tillack & Abdou (1991), Bühler (1993), Barleon *et al.* (1992, 1993*a*).

Since not all of these papers are related to the present study of flow with $\alpha = 0°$, we will focus on the most important of them.

Moon & Walker (1990), Moon et al. (1991), Hua & Walker (1991) consider a flow in a 90° bend placed in a magnetic field which is turned by $+5.71°$, by $-45°$, and by $\pm 5°$, $\pm 15°$, respectively. All walls have the same wall conductance ratio c. The $-45°$ bend is not relevant to blanket applications, but shows all the important physical aspects of a non-perfectly aligned MHD bend flow, since three-dimensional effects are most pronounced in that case. The solution leads to high velocities, $O(M^{\frac{1}{2}})$, in thin boundary layers of thickness $O(M^{-\frac{1}{2}})$ along the walls $z = \pm 1$. In a backward elbow an internal layer occurs along magnetic field lines which cross the inner corner. This layer of thickness $O(M^{-\frac{1}{2}})$ can carry a significant part of the total flow rate. For the $-45°$ case with $c = 0.1$, approximately half of the flow is carried by the internal layer and does not enter the bend section at all. In their concluding remarks Moon et al. (1991) note a decreasing flow rate carried by the internal layer as the inclination tends to zero. In addition, they predict an increasing volume flux carried by the internal layer with decreasing c. From this result they conclude that for poorly conducting or insulating channel walls the total flow will be concentrated in the internal layer. In backward elbows core velocities become small only in a narrow region at the outer corner, but the core is never stagnant, in contrast to predictions by Hunt & Holroyd or by Hunt. For forward elbows the core velocity always has components significantly different from zero.

Moon & Walker (1990) extrapolate their results, which they obtained for small values of α, to the case of $\alpha = 0°$. They conclude that the flow predicted by Hunt, with the total volume flux carried by an internal layer and further by a boundary layer at $x = 0$, does not exist for $\alpha = 0°$.

The present paper treats the flow in a U-bend with perfectly aligned toroidal duct walls, i.e. $\alpha = 0°$. The assumptions are the same as those imposed by Walker and co-authors, namely that the Hartmann number is high $(M \gg 1)$, the flow is inertialess $(N \gg M^{\frac{3}{2}})$, and the walls are much better conductors than the parabolic layers $(c \gg M^{-\frac{1}{2}})$. The last assumption allows currents conducted by the parabolic layers to be neglected so that the whole current induced in the core enters the conducting walls. As a result, the problem governing the flow in the core and the integral flow quantities, such as pressure drop, wall potential and flow partition between the core and the parabolic layers become independent of the Hartmann number. The only parameters affecting the flow are the wall conductance ratio c and the duct geometry (e.g. Hua et al. 1988; Moon & Walker 1990).

A detailed analysis shows that simple extrapolations of known solutions do not lead to a complete understanding of all possible flow structures. We can confirm the first conclusion by Moon et al. (1991) of vanishing volume flux in the internal layer only in a narrow range of the wall conduction ratio. In contrast to their second conclusion, namely increasing volume flux in the layer at $x = 0$ with decreasing c, we find the opposite tendency. We also find a strong dependence of the flow pattern on the wall conductance ratio and also on the aspect ratio d of toroidal duct cross-sections. Depending on these parameters, the flow can be of any type predicted in all papers cited. Furthermore, the flow exhibits quite unexpected and non-trivial flow patterns. In addition, a high-velocity jet occurs at the plasma-facing first wall at $x = d$ which is a novel feature of the flow considered here. This jet may play an especially important role for a toroidal blanket concept, since it is tangential to the first wall, where a high heat flux has to be removed by sufficient convective transport. The toroidal duct aspect ratio and the wall conductance ratio turn out to play a decisive role, governing the whole

problem. Since they can be used to control the flow in the toroidal coolant channels, their effect is studied in detail.

2. Formulation

Consider the steady flow of a viscous conducting incompressible fluid in a U-bend (figure 1 a). The U-bend consists of three parts:

a radial duct 1 at $x \leqslant 0$, $-1 \leqslant z \leqslant 1$, $0 \leqslant y \leqslant a$;

a radial duct 2 at $x \leqslant 0$, $-1 \leqslant z \leqslant 1$, $2l-a \leqslant y \leqslant 2l$;

a toroidal duct at $0 \leqslant x \leqslant d$, $-1 \leqslant z \leqslant 1$, $0 \leqslant y \leqslant 2l$.

All ducts have rectangular cross-sections.

A strong uniform external magnetic field $\boldsymbol{B} = B_0 \hat{\boldsymbol{y}} (\alpha = 0°)$ is aligned with the four walls of the toroidal duct, namely, $z = \pm 1$, $x = 0$, and $x = d$. The U-bend is assumed to be symmetric with respect to both $y = l$ and $z = 0$ planes, and since inertial effects are neglected, the flow in the quarter of the duct $y \leqslant l$, $z \geqslant 0$ is considered under appropriate symmetry conditions. The walls of this part of the bend are numbered from 1 to 7, as shown in figure 1(a).

The dimensionless inertialess inductionless equations governing the problem are (e.g. Moon & Walker 1990)

$$M^{-2}\nabla^2 v + j \times \hat{\boldsymbol{y}} = \nabla p, \quad j = -\nabla\phi + v \times \hat{\boldsymbol{y}}, \qquad (1\,a, b)$$

$$\nabla \cdot v = 0, \quad \nabla \cdot j = 0, \qquad (1\,c, d)$$

where the fluid velocity $v = u\hat{\boldsymbol{x}} + v\hat{\boldsymbol{y}} + w\hat{\boldsymbol{z}}$, the electric current density j, the electric potential ϕ and the pressure p are normalized by v_0 (the average fluid velocity at a cross-section $x = $ const of the radial duct 1), $\sigma v_0 B_0$, $v_0 B_0 L$ and $\sigma v_0 B_0^2 L$, respectively.

The boundary conditions at each wall are the no-slip condition

$$v = 0 \qquad (1e)$$

and the thin-wall condition

$$j \cdot \hat{n}_i = c_i \nabla_i^2 \phi_i, \qquad (1f)$$

where $\hat{n}_i$ is the normal unit vector to the wall i, into the fluid, ∇_i is the gradient in the plane of the wall; ϕ_i is the fluid potential on the wall i ($i = 1, \ldots, 7$). As the walls of the ducts are thin and the electric potential is continuous at the fluid–wall interface, the wall potential is also equal to ϕ_i.

The symmetry conditions for pressure and electric potential are

$$\phi = p = 0 \quad \text{at} \quad y = l, \qquad (1\,g, h)$$

$$\frac{\partial p}{\partial z} = \phi = 0 \quad \text{at} \quad z = 0. \qquad (1\,i, j)$$

In the radial duct, far away from the junction, the flow is fully developed. This is reflected by the conditions

$$\frac{\partial \phi}{\partial x} = \frac{\partial p}{\partial z} = \frac{\partial p}{\partial y} = 0 \quad \text{as} \quad x \to -\infty. \qquad (1\,k\text{–}m)$$

The symmetry conditions and the conditions as $x \to -\infty$ for other flow variables are not used. They can be derived from conditions (1 g–m) and the governing equations.

The fluid velocity satisfies the constant-volume-flux condition

$$\int_0^1 dz \int_0^a u\, dy = a \qquad (1n)$$

for any cross-section $x = $ const. of the radial duct and

$$\int_0^1 dz \int_0^a v\, dx = a \qquad (1o)$$

for any cross-section $y = $ const. of the toroidal duct in the region $a \leqslant y \leqslant l$.

Equations $(1a\text{--}d)$ together with conditions $(1e\text{--}o)$ constitute the problem for the flow in a U-bend. After the solution is obtained the wall currents j_i are determined from

$$j_i = -\frac{\sigma_i}{\sigma}\nabla_i\phi_i. \qquad (2)$$

3. Flow analysis at large Hartmann numbers

As $M \to \infty$, the interior of the bend may be divided into certain subregions (figure $1b, c$), where the flow is governed by the reduced equations. Most of the flow region is occupied by the inviscid cores CR in the radial duct and CT in the toroidal duct. The cores of both ducts are separated from the walls and from each other by layers of two types: the Hartmann layers H near the walls perpendicular to the magnetic field with a thickness of $O(M^{-1})$; the parabolic layers parallel to the magnetic field with $O(M^{-\frac{1}{2}})$ thickness.

The latter occur at the sidewalls of both ducts (regions SR and ST), the first wall (region F), the second wall (region S), and inside the fluid at the junction $x = 0$ (internal layer, region I). At $y = a$ layers I and S merge, and therefore they must be treated simultaneously.

Near the corners $z = 1$, $x = d$ and $z = 1$, $x = 0$, where layers ST and SR intersect with layers F, S, and I, layers $A1$ and $A2$ are formed with x- and z-dimensions both of $O(M^{-\frac{1}{2}})$. The flow in layers $A1$ and $A2$ is governed by a system of two-dimensional convective heat conduction equations, and therefore they may be called two-dimensional parabolic layers. Similar to the core regions, parabolic layers are separated from the walls perpendicular to the field by the Hartmann layers.

In addition, there are inner corner regions with $O(M^{-1}) \times O(M^{-1})$ dimensions at the corners adjacent to the tops and bottoms of all ducts. These regions are of no interest here because they carry no $O(1)$ volume flux and have no influence on the flow structure to the main order in the other subregions (Cook, Ludford & Walker 1972).

3.1. Core regions

In the core regions viscous terms in $(1a)$ may be neglected. This corresponds to the limit $M \to \infty$. The general solution of the resulting equations is (Moon & Walker 1990)

$$u_C = \frac{\partial\phi_C}{\partial z} - \frac{\partial p_C}{\partial x}, \quad v_C = y\left[\frac{\partial^2 p_C}{\partial x^2} + \frac{\partial^2 p_C}{\partial z^2}\right] + g_1, \quad w_C = -\frac{\partial\phi_C}{\partial x} - \frac{\partial p_C}{\partial z}, \qquad (3a\text{--}c)$$

$$j_{xC} = \frac{\partial p_C}{\partial z}, \quad j_{yC} = -\frac{\partial\phi_C}{\partial y}, \quad j_{zC} = -\frac{\partial p_C}{\partial x}, \qquad (3d\text{--}f)$$

$$\phi_C = g_2 + g_3 y, \qquad (3g)$$

where $p_C(x, z)$ is the core pressure; $g_n(x, z)$ $(n = 1\text{–}3)$ are integration functions. Throughout this paper subscripts of flow variables denote the flow subregion, where corresponding limit equations are valid. Subscript C denotes both CT and CR.

The jumps in the component of electric current normal to the wall across the Hartmann layers and parabolic layers are at most $O(M^{-1})$ and $O(M^{-\frac{1}{2}})$, respectively. The jump of the potential across the Hartmann layers is at most $O(M^{-2})$. Neglecting these jumps has the following consequences.

(i) The normal component of the core velocity vanishes at the Hartmann walls of both ducts, i.e.

$$v_{CR} = 0 \quad \text{at} \quad y = 0 \quad \text{and at} \quad y = a, \quad x \leqslant 0; \tag{4a}$$

$$v_{CT} = 0 \quad \text{at} \quad y = 0, \quad x \geqslant 0. \tag{4b}$$

(ii) The core current satisfies the thin-wall conditions $(1f)$ at all walls, i.e.

$$\boldsymbol{j}_C \cdot \hat{\boldsymbol{n}}_i = c_i \nabla_i^2 \phi_i \quad \text{at wall } i \quad (i = 1, \dots, 7). \tag{4c}$$

(iii) The core potentials, estimated at walls 4, 6, and 7, are equal to the potentials of these walls, i.e.

$$\phi_C = \phi_i \quad \text{at wall } i \quad (i = 4, 6, 7). \tag{4d}$$

3.1.1. *Core of the radial duct 1*

By substituting (3) into $(4a, c, d)$ the unknown functions g_n are determined which gives expressions for the core-flow variables in the radial duct in terms of wall potentials and core pressure, namely

$$u_{CR} = -\frac{\partial p_{CR}}{\partial x} + \left(1 - \frac{y}{a}\right)\frac{\partial \phi_7}{\partial z} + \frac{y}{a}\frac{\partial \phi_6}{\partial z}, \quad v_{CR} = 0, \tag{5a, b}$$

$$w_{CR} = -\frac{\partial p_{CR}}{\partial z} + \left(\frac{y}{a} - 1\right)\frac{\partial \phi_7}{\partial x} - \frac{y}{a}\frac{\partial \phi_6}{\partial x}, \quad \phi_{CR} = \phi_6 + \left(1 - \frac{y}{a}\right)(\phi_7 - \phi_6), \tag{5c, d}$$

$$j_{xCR} = \frac{\partial p_{CR}}{\partial z}, \quad j_{yCR} = a^{-1}(\phi_7 - \phi_6), \quad j_{zCR} = -\frac{\partial p_{CR}}{\partial x}, \tag{5e–g}$$

and lead to the equations

$$c_5 \nabla_5^2 \phi_5 = \frac{\partial p_{CR}}{\partial x}(x, z = 1), \quad c_7 \nabla_7^2 \phi_7 = a^{-1}(\phi_7 - \phi_6), \quad c_6 \nabla_6^2 \phi_6 = -a^{-1}(\phi_7 - \phi_6), \tag{6a–c}$$

$$\frac{\partial^2 p_{CR}}{\partial x^2} + \frac{\partial^2 p_{CR}}{\partial z^2} = 0. \tag{6d}$$

In the radial duct the volume flux in the x-direction is carried by the core CR and the side layer SR, so that it is a sum of the volume fluxes $Q_{CR, x}$ and $Q_{SR, x}$, which are

$$Q_{CR, x} = -a \int_0^1 \frac{\partial p_{CR}}{\partial x} \, \mathrm{d}z + \tfrac{1}{2}a[\phi_6(x, z = 1) + \phi_7(x, z = 1)]; \tag{7a}$$

$$Q_{SR, x} = \int_0^a \phi_5(x, y) \, \mathrm{d}y - \tfrac{1}{2}a[\phi_6(x, z = 1) + \phi_7(x, z = 1)]. \tag{7b}$$

Expression (7*b*) is obtained by the integration of the *z*-component of Ohm's law across layer *SR* (e.g. Moon & Walker 1990). Substituting (7*a*) and (7*b*) into the (1*n*) gives the condition

$$\int_0^a \phi_5(x, y)\, \mathrm{d}y - a \int_0^1 \frac{\partial p_{CR}}{\partial x}(x, z)\, \mathrm{d}z = a. \tag{6e}$$

3.1.2. *Core of the toroidal duct CT*

Substituting (3) into (4*b–d*) and the symmetry conditions (1*g, h*) gives the equations governing the wall potentials of the toroidal duct, namely

$$\nabla_1^2 \phi_1 = \nabla_2^2 \phi_2 = \nabla_3^2 \phi_3 = 0, \quad lc_4 \nabla_4^2 \phi_4 = \phi_4. \tag{8a–d}$$

The core variables are expressed in terms of wall potentials as follows:

$$\phi_{CT} = \left(1 - \frac{y}{l}\right)\phi_4, \quad p_{CT} = 0; \quad u_{CT} = \frac{\partial \phi_{CT}}{\partial z} = \left(1 - \frac{y}{l}\right)\frac{\partial \phi_4}{\partial z}; \tag{9a–c}$$

$$v_{CT} = 0; \quad w_{CT} = -\frac{\partial \phi_{CT}}{\partial x} = -\left(1 - \frac{y}{l}\right)\frac{\partial \phi_4}{\partial x}; \tag{9d, e}$$

$$j_{xCT} = 0, \quad j_{yCT} = \frac{1}{l}\phi_4, \quad j_{zCT} = 0. \tag{9f–h}$$

Consider now the boundary conditions for (6) and (8). If the walls *i* and *k* have a common boundary Γ_{ik}, the continuity of the potential and the normal component of current density requires that

$$\phi_i = \phi_k, \quad c_i \frac{\partial \phi_i}{\partial \hat{s}_i} = -c_k \frac{\partial \phi_k}{\partial \hat{s}_k} \quad \text{at} \quad \Gamma_{ik}, \tag{10a, b}$$

where $\hat{s}_i$, $\hat{s}_k$ are outward normal unit vectors to Γ_{ik} in the planes of the walls *i* and *k*, respectively.

Conditions (1*k, l*) of fully developed flow at infinity in the radial duct give

$$\frac{\partial \phi_5}{\partial x} = \frac{\partial \phi_6}{\partial x} = \frac{\partial \phi_7}{\partial x} = \frac{\partial p_{CR}}{\partial z} = 0. \tag{10c–f}$$

Condition (1*m*) is automatically satisfied by the function p_{CR}.

The symmetry conditions (1*g–j*) give

$$\frac{\partial p_{CR}}{\partial z} = \phi_1 = \phi_2 = \phi_4 = \phi_6 = \phi_7 = 0 \quad \text{at} \quad z = 0, \tag{10g–l}$$

$$\phi_1 = \phi_2 = \phi_3 = 0 \quad \text{at} \quad y = l. \tag{10m–o}$$

Subject to conditions (10), the system of equations (6) and (8) is solved numerically. After the solution is obtained, the flow in the core is reconstructed using (5) and (9). Condition (1*o*) has not been used to derive (8). It will be shown in §3.3 that it is satisfied automatically.

Equations (5*b*) and (9*d*) indicate that in both cores the velocity component parallel to magnetic field lines is zero. For the toroidal duct this result means that the core does not carry a volume flux, so that the whole volume flux is carried by high-velocity jets in the parabolic layers *ST*, *F*, *I* and *S*.

Expression (9d) was obtained by using the condition (4a) of matching the Hartmann-layer variables, the symmetry condition (1h) for pressure, and the facts that the core pressure does not vary along magnetic field lines, and the y-component of core velocity is a linear function of y. Relation (9d) holds for any wall conductance ratio of the bottom, including the case of insulating walls, because condition (4b) at the boundary of the Hartmann layer is valid for an arbitrary wall conductance ratio. It holds also for non-symmetric U-bends, because the symmetry condition for pressure at $y = l$ may be replaced by the condition on the top of the toroidal duct which is analogous to (4b). This means that if the magnetic field is perfectly aligned with the walls of the toroidal duct, its core does not carry a volume flux in the y-direction, and the only possibility of removing heat from the first wall of the blanket consists in generating a high-velocity jet in layer F. Thus, the local flow structure in layer F is important, since it determines the conditions of cooling the first wall. This layer is treated in detail in §3.2. The other layers are treated integrally, because they are of minor importance.

3.2. *Layer F*

Order-of-magnitude arguments show that in layer F the functions v and w are of $O(M^{\frac{1}{2}})$; ϕ, j_z, j_y are of $O(1)$; p and j_x are of $O(M^{-\frac{1}{2}})$. The equations governing the flow in layer F are

$$\frac{\partial^2 v_F}{\partial \xi^2} = \frac{\partial p_F}{\partial y}; \quad \frac{\partial^2 p_F}{\partial \xi^2} = \frac{\partial v_F}{\partial y}; \quad \frac{\partial^4 \phi_F}{\partial \xi^4} = \frac{\partial^2 \phi_F}{\partial y^2}; \qquad (11a\text{–}c)$$

where $\xi = M^{\frac{1}{2}}(x - d)$ is the boundary-layer coordinate. Once the solution is found, the other flow variables are determined from

$$u_F = -\frac{\partial p_F}{\partial \xi} + \frac{\partial \phi_F}{\partial z}; \quad w_F = -\frac{\partial \phi_F}{\partial \xi}, \qquad (12a, b)$$

$$j_{xF} = -\frac{\partial p_F}{\partial z} + \frac{\partial^3 \phi_F}{\partial \xi^3}; \quad j_{yF} = -\frac{\partial \phi_F}{\partial y}; \quad j_{zF} = -\frac{\partial p_F}{\partial \xi}. \qquad (12c\text{–}e)$$

No-slip conditions and the continuity of the electric potential at walls 1 and 4, the symmetry conditions at $y = l$, and conditions of matching the core variables give

$$v_F = 0, \quad \frac{\partial p_F}{\partial \xi} = \frac{\partial \phi_1}{\partial z}, \quad \phi_F = \phi_1, \quad \frac{\partial \phi_F}{\partial \xi} = 0 \quad \text{at} \quad \xi = 0, \qquad (11d\text{–}g)$$

$$v_F = 0, \quad \phi_F = \phi_4(x = d, z) \quad \text{at} \quad y = 0; \qquad (11h, i)$$

$$\frac{\partial v_F}{\partial y} = 0, \quad \phi_F = 0 \quad \text{at} \quad y = l; \qquad (11j, k)$$

$$v_F \to 0, \quad \frac{\partial p_F}{\partial \xi} \to 0, \quad \phi_F \to \phi_4(x = d, z) \quad \text{as} \quad \xi \to -\infty. \qquad (11l\text{–}n)$$

A solution to problem (11) can be obtained in terms of Fourier series. For example, the y-component of velocity is

$$v_F = \sum_{n=0}^{\infty} e^{-\gamma_n \xi} \delta_n \sin \gamma_n \xi \sin \beta_n y, \qquad (13)$$

where $\qquad \delta_n = \frac{2}{l\gamma_n} \int_0^l \frac{\partial \phi_1}{\partial z} \cos \beta_n y \, dy; \quad \beta_n = (n + \frac{1}{2}) \frac{\pi}{l}; \quad \gamma_n = (\frac{1}{2}\beta_n)^{\frac{1}{2}}.$

In flows in complex geometries the local flow structure in parabolic layers is usually difficult to analyse because of problems intractable by analytical methods. Examples in the present flow are layers I and S. The most essential information about the local flow structure can be obtained by considering local flow rates within a parabolic layer.

Consider an infinitesimal element dV within layer F, formed by planes y, $y+dy$, z, $z+dz$. Integration of the mass conservation equation with respect to ξ over the layer gives

$$u_{CT}(x = d, z) = \frac{\partial}{\partial y} q_{F,y}(y,z) + \frac{\partial}{\partial z} q_{F,z}(y,z), \tag{14}$$

where
$$q_{F,y}(y,z) = \int_{-\infty}^{0} v_F \, d\xi = \int_0^y \frac{\partial \phi_1}{\partial z} \, dy = -\frac{1}{c_1} \int_0^y j_{1,z} \, dy, \tag{15}$$

$$q_{F,z}(y,z) = \int_{-\infty}^{0} w_F \, d\xi = \left(1 - \frac{y}{l}\right) \phi_4(x = d, z) - \phi_1(y,z) \tag{16}$$

are local flow rates carried by the layer in the y- and z-directions, respectively. Expression (15) is obtained by integrating (11b) with respect to ξ and y.

The total volume flux $Q_{F,y}$ carried by layer F in the y-direction is

$$Q_{F,y} = \int_0^y \phi_1(y, z = 1) \, dy = -\frac{1}{c_1} I_{1z}, \tag{17}$$

where I_{1z} is the z-component of total current in the first wall, integrated over the distance y from the bottom and averaged over z.

The average velocity $U_{CT,F}$ of the fluid entering layer F from the core at a cross-section $y = $ const. is obtained by integrating (9c) with respect to z to give

$$U_{CT,F} = \left(1 - \frac{y}{l}\right) \phi_4(x = d, z = 1). \tag{18}$$

At the corner $A1$ part of the fluid leaves layer F with local flow rate $q_{F,z}(y, z = 1)$.

3.3. *Layers ST, S and I*

The equations governing the flow in layers ST and the boundary conditions are similar to those in layer F. Local flow rates in layer ST are

$$q_{ST,y}(x,y) = -\int_0^y \frac{\partial \phi_3}{\partial x} \, dy = \frac{1}{c_3} \int_0^y j_{3,x} \, dy, \tag{19}$$

$$q_{ST,x}(x,y) = \phi_3(x,y) - \left(1 - \frac{y}{l}\right) \phi_4(x, z = 1). \tag{20}$$

The total flow rate carried by layer ST in the y-direction is

$$Q_{ST,y} = \int_0^y [\phi_3(x = 0, y) - \phi_3(x = d, y)] \, dy. \tag{21}$$

The average velocity of the fluid entering layer ST from the core CT at the cross-section $y = $ const. is

$$W_{ST,CT} = -(1 - y/l)[\phi_4(x = d, z = 1) - \phi_4(x = 0, z = 1)]. \tag{22}$$

The equations governing the flow in layers S and I are exactly the same as those in layer F with $\xi = M^{\frac{1}{2}}x$. The only essential information about these layers is the flow rates $Q_{S,y}$ and $Q_{I,y}$ carried by them in the y-direction:

$$Q_{S,y} = a - \int_0^y \phi_3(x = 0, y) \, dy, \tag{23}$$

$$Q_{I,y} = -y \int_0^1 \frac{\partial p_{CR}}{\partial x}(x = 0, z) \, dz. \tag{24}$$

These flow rates are obtained in the same way as (17) for $Q_{F,y}$. In the region $y < a$, i.e. in layer I, (11b) is integrated over the region $-\infty < \xi < \infty$, and instead of the boundary conditions at wall 2, conditions of matching with the core variables in the radial duct are applied. The sum of the three flow rates $Q_{F,y}$, $Q_{S,y}$ and $Q_{ST,y}$ gives the value of a so that condition (1o) is satisfied automatically.

The amount of fluid leaving layer F at a cross-section $y =$ const. at corner $A1$ is equal to that entering layer ST, since $q_{ST,x}(x = d, y) = -q_{F,z}(y, z = 1)$. This means that layer $A1$ does not carry $O(1)$ volume flux, and its role it to match a possible jump in the $O(M^{\frac{1}{2}})$ y-component of velocity at the corner. The same conclusion applies to the intersection of layers ST and S at corner $A2$.

In the region $0 \leqslant y \leqslant a$ at corner $A2$ three layers intersect, namely SR, ST and I, and this region requires special attention. The amount of fluid leaving layer SR at $x = 0$ is given by (7b). The amount of fluid entering layer ST at $x = 0$ is obtained by the integration of (20) to give

$$Q_{ST,x}(x = 0) = \int_0^a \phi_3(x = 0, y) \, dy - a\left(1 - \frac{a}{2l}\right)\phi_4(x = 0, z = 1). \tag{25}$$

The difference between the first and second flow rates is

$$\Delta Q_{SR,ST} = \tfrac{1}{2}a\{((a/l) - 1)\,\phi_4(x = 0, z = 1) + \phi_6(x = 0, z = 1)\}. \tag{26}$$

However, this difference does not lead to $O(1)$ volume flux in layer $A2$ in the y-direction. The deficit is taken from layer I, since integration of (12b) across layer I gives the expression $-\Delta Q_{SR,ST}$.

4. Results and discussion

The system of equations (6), (8) has been solved numerically by two different methods. The first is an iterative method with iterations between equations for wall potentials and core pressure. The second method is a general one for the solution of core-flow equations in curvilinear coordinates generated by the channel geometry and magnetic field orientation. The second, general, method has been successfully applied to a number of complex flow geometries and in particular to the flow in a backward elbow with $\alpha = -15°$ (see Bühler 1993, who for this case also presents a comparison with an experiment). The first method was specially developed for this particular problem, which is singular in a sense for the second method. The reason for this singularity lies in the perfect alignment of the toroidal duct and the magnetic field that is impossible to simulate exactly with the second method. To overcome this difficulty, toroidal duct walls are slightly inclined with respect to the magnetic field in the second method. This leads to a stretched grid in the y-direction and, consequently, to some

disagreement between the two methods for $l > 4$. For a detailed description of the methods and a comparison between the results see Molokov & Bühler (1993). Here we present results obtained by the first method. Calculations were done on a grid with 32 points per unit length in each direction. The length of the radial duct was 10. This length was sufficient to reach fully developed conditions at the entrance in all calculations presented here. Iterations stopped when the differences in nodal pressures and wall potentials in two subsequent steps were less than 0.1%.

4.1. *Reference case*

In the reference case, for which results are presented first, square cross-sections are assumed for both ducts ($a = 2$, $d = 2$), the same wall conductance ratio $c = 0.2$ for all walls, and $l = 12$, i.e. the length of the toroidal duct $2l = 24$. The values of c and l are close to the wall conductance ratio of the first wall and to the half-length of the toroidal duct of the radial–toroidal–radial blanket concept, respectively. Throughout §4 these values are default unless otherwise stated explicitly.

In §3 the magnetohydrodynamic flow problem has been reduced to the 'electric' one. The only hydrodynamic variable which enters reduced governing equations is the core pressure in the radial duct. It provides an initial electric current source, equal to $\partial p_{CR}/\partial x(x, z = 1)$, the x-component of the local pressure gradient estimated at sidewall 5. This current 'charges' the walls, which constitute an electric circuit. Thus, the hydrodynamic part of the problem follows the rules prescribed by the electrical properties of the walls. Hence, we first describe electric current paths and then consider their influence on the flow structure.

In radial duct 1, far from the junction, the flow is fully developed. It is unidirectional, and none of the variables, except for pressure, varies with x, the coordinate in the main flow direction. In the radial duct an electrically conducting fluid flows perpendicular to the magnetic field lines. Hence, an electric current is induced initially in the z-direction. The value of this current is determined by the core velocity and is equal (in non-dimensional terms) to the pressure gradient. Since in a fully developed flow the pressure gradient is constant, the core current is uniform; it flows in the z-direction only and enters sidewall 5 at $z = 1$. The electric current induces a potential difference between any two points with different values of z, and therefore between the sidewalls at $z = \pm 1$ as well. This induced voltage drives electric currents inside the walls. In the region of fully developed flow no voltage is induced in the x-direction. Hence, the current entering the sidewall at $z = 1$ completes its circuit in the top (or the bottom) and the other sidewall at $z = -1$ in planes $x = $ const., i.e. perpendicular to the main flow direction. For this reason, we call this current two-dimensional. Owing to the symmetry with respect to the plane $y = \frac{1}{2}a$, the top and bottom potentials are equal.

In radial duct 2 the flow direction is opposite to that in duct 1, so that the current changes direction, and the induced voltage is of opposite sign. As a result, an antisymmetric potential distribution with respect to $y = l$ appears both inside the fluid and along the walls. This voltage drives three-dimensional electric currents from the first part ($y < l$) to the second part ($y > l$) of a U-bend for $z > 0$, and back for $z < 0$. Isolines of wall potential at $y < l$ are shown in figure 2. Since wall currents are proportional to the gradient of the wall potential (equation (2)), electric current lines are perpendicular to the isolines at each point.

In radial duct 1, close to the junction between that duct and the toroidal duct, the current loop loses its symmetry with respect to $y = \frac{1}{2}a$ because of induced three-dimensional voltage. The measure of this non-symmetry is the difference between the potentials of the top and bottom. The latter results in the current j_{yCR} (equation
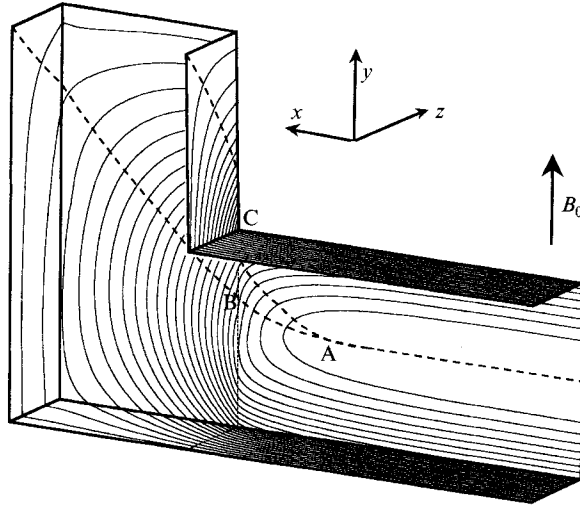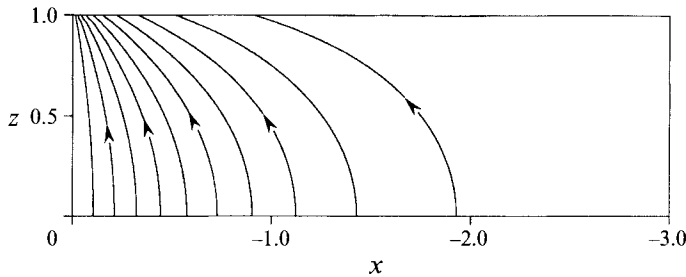
FIGURE 2. Isolines of wall potential.

FIGURE 3. Projection of three-dimensional electric current lines on (x, z)-plane. These are isolines of three-dimensional pressure in the radial duct.

$(5f)$). Therefore, in the radial duct, near the junction all three components of core current are non-zero. However, in the toroidal duct, components of current perpendicular to the field (j_{xC_T} and j_{zC_T}) are both zero. The amount of current that can be conducted by the internal layer is of the order of $M^{-\frac{1}{2}}$; it is negligible compared to the core current. As a result, there is no current path from the radial to the toroidal duct inside the fluid to the main order. Hence, all current induced in the radial duct must enter its walls. The magnitude of the induced current is determined by the conductance of the electric circuit. If there were a closed current loop inside the core, the induced current would be of the order 1, the conductance of the core. Since the whole current enters the walls, it is of the order of the wall conductance ratio. For low values of c both the induced current and thus the pressure drop are small. Figure 3 shows lines of three-dimensional core current in the radial duct in the planes perpendicular to the magnetic field. In the radial duct this current represents the deviation from the current distribution for fully developed flow. The current in figure 3 enters sidewall 5 at $z = 1$. However, since there is a positive y-component of three-dimensional current at $z > 0$, part of the current lines enter the top 6 of radial duct 1, and then close the loop in the region $z < 0$, or even enters wall 2 from wall 6 before crossing the plane $z = 0$. However, a much larger amount of current generally follows two main paths (figure 2).

The first path is associated with the current that does not cross the symmetry plane $y = l$, and is confined to the part $y < l$. For this reason, we call this path a short one. It involves current that enters sidewall 5 outside the curvilinear triangle ABC in figure 2, crosses the junction $x = 0$, enters sidewall 3 of the toroidal duct, and then closes through walls 1, 2, or 4. Owing to the symmetry, there is another short path at $y > l$. Two short paths are isolated from each other by the symmetry plane $y = l$.

Current lines that enter the triangle ABC belong to the second, long path. It is associated with the current crossing the symmetry plane $y = l$ along walls 1, 2, or 3. Part of the wall current that enters the bottom 4 may leave it into the core CT, flow along magnetic field lines and cross the symmetry plane $y = l$ within the fluid, so that this part of the current also belongs to the long path. The current that crosses the plane $y = l$ at $z > 0$, returns to radial duct 1 at $z < 0$ after full circulation in the duct $y > l$, i.e. after crossing the symmetry plane $z = 0$ in radial duct 2. The portions of current that belong to the short and long paths depend on the resistance of the small and big electric circuits. The influence of flow parameters on the resistance will be discussed later.

In the toroidal duct the pressure is equal to zero to the main order. This supports the idea of aligning the field to the first-wall coolant channels where high velocity of the coolant is required. However, the pressure drop in the radial duct increases with respect to that in a pure fully developed flow, because three-dimensional currents cause an additional electromagnetic force, which must be balanced by an increased level of the core pressure. The isolines of three-dimensional pressure in radial duct 1 are shown in figure 3. To characterize the value of the three-dimensional pressure losses, Hua & Walker (1991) introduce the so-called three-dimensional length d_{3D}, which for the present geometry is

$$d_{3D} = \frac{\Delta p_{3D}}{\partial p_{CR}/\partial x(x \to -\infty)},$$

where Δp_{3D} is the three-dimensional pressure drop and $\partial p_{CR}/\partial x(x \to -\infty)$ is the fully developed pressure gradient in the radial duct, which for $c_6 = c_7$ can be estimated using the well-known formula $[1 + 2a/c_6 + (a^2/12c_5)]^{-1}$ (e.g. Hua $et\ al.$ 1988; Moon & Walker 1990). It should be noted that owing to the assumption $c \gg M^{-\frac{1}{2}}$ this formula fails as $c \to 0$. Δp_{3D} is the difference between the total pressure drop and that for fully developed flow estimated over such a length in the radial duct that fully developed flow conditions are established. With such a definition three-dimensional pressure losses are characterized by the additional length of the radial duct d_{3D} with a fully developed flow. As was pointed out by Walker and co-authors (Moon & Walker 1990; Hua $et\ al.$ 1991; Hua & Walker 1991), the three-dimensional pressure drop in bends is small. It is equivalent to the extension of the radial duct by about one characteristic length (Hua & Walker 1991). Present calculations of the three-dimensional pressure drop in a U-bend for a wide range of flow parameters confirm this conclusion. In the reference case $\Delta p_{3D} = -0.1063$, $\partial p_{CR}/\partial x(x \to -\infty) = -0.1304$, so that $d_{3D} = 0.8152$, which is small compared to the typical length of the radial duct $(2 < l_{RAD} < 6)$. However, if the walls of the toroidal duct are much better conductors than those of the radial duct, the three-dimensional length reaches much higher values. In the extreme case of perfectly conducting walls of the toroidal duct, $d_{3D} = 3.91$. In this case, three-dimensional effects contribute considerably to the total pressure drop. The three-dimensional length is also much higher if the aspect ratio $\frac{1}{2}a$ of the radial duct is small.

Another characteristic of three-dimensional effects is the development length, i.e. the distance from the junction where the flow becomes fully developed. Figures 3 and 4
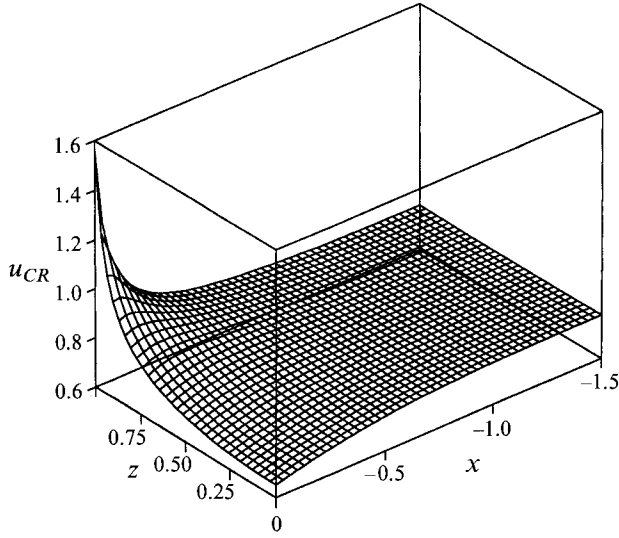
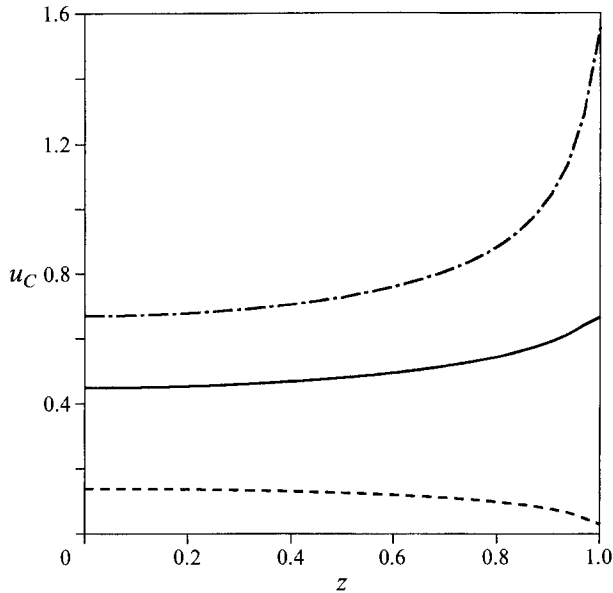FIGURE 4. Axial component of core velocity u_{CR} in the radial duct at $y = \frac{1}{2}a$.

FIGURE 5. Profiles of x-component of core velocity u_{CR} for $x = -0$ (———·———·———) and u_{CT} for $x = +0$ (————), $x = d$ (————) at $y = 0$.

indicate that the development length in the radial duct is about 1, in contrast to the toroidal duct, where the development length is very high (see discussion further in the text).

Consider now the effect of three-dimensional currents on the flow structure. In radial duct 1, far upstream, the flow is fully developed. The volume flux is carried by the core (78%) and the side layers (22%) at both sidewalls, in accordance with Tillack & McCarthy (1989). The core velocity is uniform (figure 4). When the fluid approaches the junction, three-dimensional currents change the velocity profile. In the centre of the radial duct the z-component of the three-dimensional current is stronger than at the
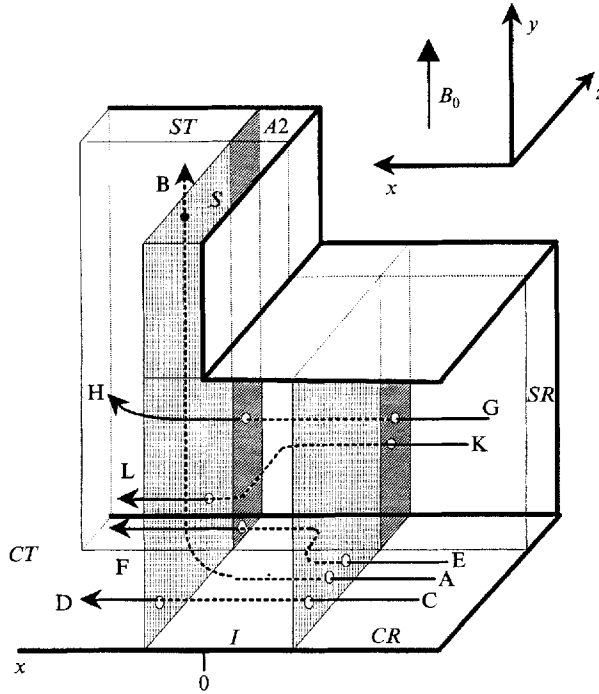
FIGURE 6. Flow redistribution at the junction $x = 0$.

sidewalls, because current lines turn in the direction of the junction (figure 3). As a result, the axial component of the core velocity becomes smaller in the centre than at the sidewalls. The x-component of the current causes fluid flow from the core towards the side layers, and hence streamlines in the core deviate from being straight and turn in the direction of the side layers. The volume flux carried by the layers at the junction slightly increases, by 1%, and that carried by the core decreases. The difference between the potentials of the top 6 and the bottom 7 results in a linear variation with y of the axial component of the core velocity, with higher velocity at the top. However, qualitatively the flow structure is the same as in a straight duct with a non-uniform magnetic field (Hua et al. 1988). The flow redistribution in the toroidal duct is more dramatic.

When the fluid approaches the toroidal duct from the core CR, it first meets internal layer I, across which jumps in the x- and z-components of the core velocity occur (figure 5 and equations (5a, c) and (9c, e)). In layer I the core volume flux generally splits up into three parts (figure 6). The first part (path AB) is carried in the y-direction as a high-velocity jet by the internal, and then by the second-wall layer (regions I and S). The second part (CD) crosses the internal layer and enters the core of the toroidal duct. The third part turns in the direction of the sidewall, and then enters the side layer ST (EF). The last fluid path exists only if $\Delta Q_{SR,ST} < 0$, i.e. more fluid enters layer ST than leaves layer SR. This flow path is present if for example wall 6 is a perfect conductor and $l > a$.

If the fluid approaches the toroidal duct from layer SR, it enters layer ST, and then part of the fluid turns in the y-direction inside this layer (GH). If $\Delta Q_{SR,ST} > 0$, another part of the fluid carried by layer SR turns in layer I in the $-z$-direction and then enters the core CT (KL). This flow path is present for example in a 180° bend or in a U-bend with perfectly conducting wall 7.
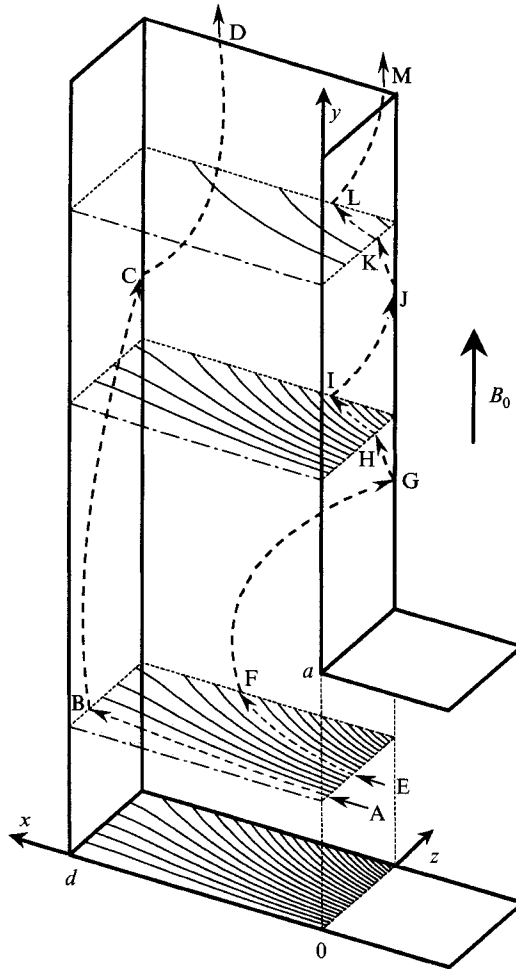
FIGURE 7. Isolines of bottom potential ϕ_4 and sketch of streamlines in the toroidal duct.

Since the y-component of the core velocity is zero in the toroidal duct, the fluid flows in planes $y = $ const., following isolines of the bottom potential 4 (equations (9c) and (9e)) which are shown in figure 7. The isolines enter the vicinity of walls 1 and 3, where layers F and ST occur. Thus the bottom potential governs the flow in the core CT and distributes the fluid between layers F and ST. Figure 5 shows the x-component of the core velocity on the bottom 4 at $x = d$ and at the junction $x = \pm 0$. The velocity is higher at the junction at $x = +0$ than at the first wall, because part of the core volume flux enters layer ST.

The amount of fluid entering layer F from the core CT is determined by the difference between values of the bottom potential ϕ_4, estimated at the sides $z = \pm 1$ (equation (18)). This means that the core of the toroidal duct acts like an electromagnetic pump. The pump takes part of the volume flux from the core of the radial duct through the internal layer I and distributes it between layers F and ST. The pumping 'power' is determined by the bottom potential. The leading role of the bottom potential, and thus the pumping effect in the core, are not restricted only to the region $y < a$, but extend to the whole core CT. If $y < a$, the fluid is taken from the radial duct, whereas in region $a < y < l$ the fluid is taken from layer S. As a result, if
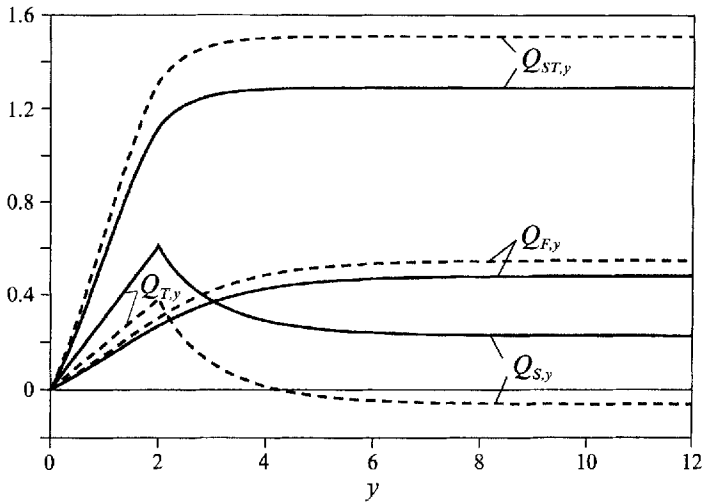
FIGURE 8. Volume fluxes carried by layers F, ST, S and I in the y-direction for $c = 0.2$ (———) and $c = 0.1$ (———). The total volume flux is 2.

the volume flux carried by layer I increases with y in region $y < a$, then in region $a < y < l$ the volume flux carried by layer S decreases with y (figure 8). The volume fluxes carried by layers F and ST monotonically increase with y. Thus, the flow distribution between layers in the toroidal duct is non-uniform in the y-direction. It changes from one cross-section $y = $ const. to the other.

It is remarkable that to order 1, in the core of the toroidal duct the flow is force-free. This is quite an unusual situation not only in conventional hydrodynamics, but also in magnetohydrodynamics. All forces in the equation of motion vanish. Nevertheless, the fluid flow obeys Ohm's law in order to compensate the potential difference induced by currents in the radial duct, representing the driving mechanism for the fluid motion in the toroidal duct.

The description of the flow structure in the toroidal duct is still incomplete, because there is mass exchange between the parabolic layers through corners $A1$ and $A2$. It is determined by the local flow rates $q_{F,z}(y, z = 1)$ and $q_{ST,x}(y, x = d)$ (figure 9). In region $y < a$ there is a non-zero volume flux from layer SR and the internal layer I into layer ST. This flow is so intensive that it passes layer ST along sidewall 3, reaches layer F and enters it from corner $A1$. This stream competes with the tendency of the fluid, which entered layer F from the core CT, to leave layer F at corner $A1$. To prove that such tendency exists, equation (18) is integrated with respect to y to give the total amount of fluid entering layer F from the core. The result is $0.5l\phi_A(x = d, z = 1)$. If l increases, this quantity becomes unlimited so that part of the fluid must leave layer F. However, in region $y < a$ the flow from layer ST into layer F is more intensive.

In region $a < y < l$, where there is no flux into layer ST from the radial duct, the mass exchange through the corners reverses sign. Part of the flow entering layer F turns and enters layer ST. Thus, in this region streamlines in layer F deviate to a certain extent from being aligned wth the field, with inclination in the direction of the sidewalls (streamline BC in figure 7). The same applies to corner $A2$, where part of the fluid leaves layer ST and enters layer S. In layer ST streamlines are inclined in the direction of wall 2 (CD).

The streamline EFG in figure 7 is associated with the fluid that leaves layer I (or S) and returns back to it, making in this sense a complete cycle. It first enters the core of
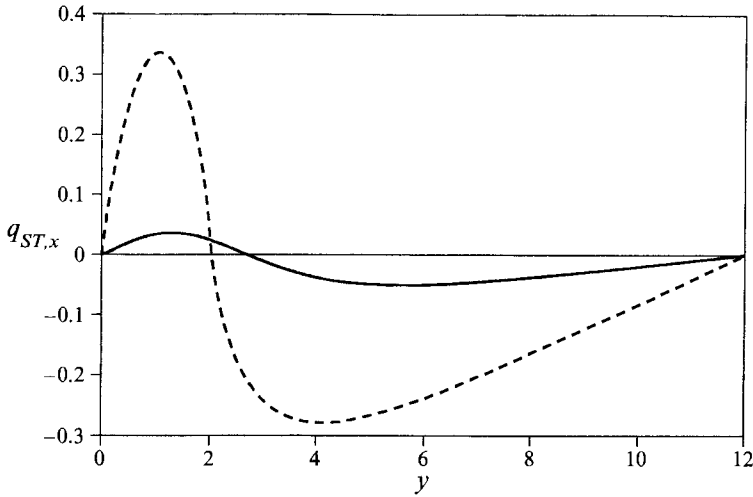
FIGURE 9. Mass exchange between parabolic layers at corners $A1$ and $A2$. Local flow rates $q_{ST,x}(x = 0, y)$ (–––) and $q_{ST,z}(x = d, y) = -q_{F,z}(y = 1)$ (——) entering layers ST and F at corners $A1$ and $A2$, respectively.

the toroidal duct from layer I (or S), enters layer ST, flows in the latter at a certain angle to the magnetic field in the direction of wall 2, and finally enters layer S. If the toroidal duct is long enough, this cycle may be repeated again (GHIJ and JKLM) which means that in the toroidal duct part of the fluid participates in a kind of helical motion. The number of cycles depends on all parameters of the flow, but especially on the length of the toroidal duct. Layer F may also be involved in the helical motion. Figures 7 and 8 indicate that more fluid enters side layer ST than layer F from the core CT. This part of the fluid participates more intensively in a helical motion, and needs only a short distance to complete the cycle.

However, not all the fluid takes part in the helical motion. There is a well-defined set of streamlines, namely those in the symmetry plane $z = 0$, which do not turn in the z-direction, because the z-component of velocity on the symmetry plane vanishes. In the part $z < 0$ there is another spiral with opposite sign of the z-component of velocity. The two spirals do not interact, because streamlines cannot cross the symmetry plane $z = 0$.

Therefore, in the toroidal duct the fluid takes part in a complicated motion with 'slow' $O(1)$ motion in the core in the planes $y = $ const., and 'jumps' or very fast $O(M^{\frac{1}{2}})$ motion in the layers. There is a mass exchange between layers through corner regions. We conclude that:

(i) there is a high-velocity jet at the first wall, which carries 24.1% of the total volume flux in the symmetry plane $y = l$;

(ii) the core is not stagnant although the velocity component in the main flow direction vanishes;

(iii) there is a mixing of fluid due to mass exchange between the layers.

All of these flow features should lead to favourable heat-transfer conditions.

4.2. *Influence of parameters on flow structure*

If the distance d between walls 1 and 2 is reduced and other parameters are fixed, a larger amount of current closes through wall 1. The three-dimensional pressure drop increases, because the resistance of the electric circuit decreases (table 1). The volume
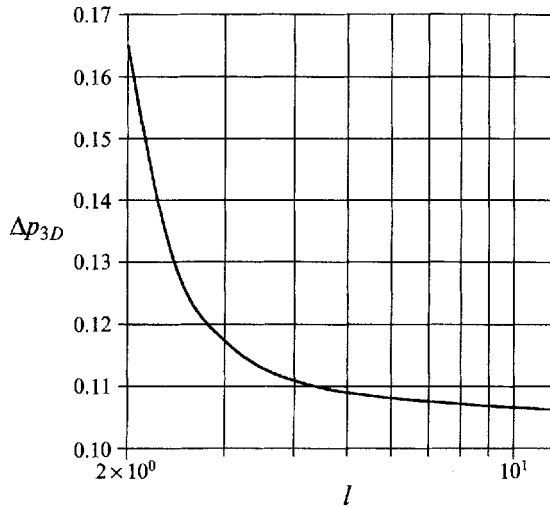
FIGURE 10. Variation of Δp_{3D} with l.

d	Δp_{3D}	$Q_{F,y}(y=l)$	$Q_{ST,y}(y=l)$	$Q_{S,y}(y=l)$
2.000	−0.1063	0.482	1.290	0.228
1.500	−0.1080	0.608	1.130	0.262
1.000	−0.1109	0.788	0.902	0.310
0.500	−0.1161	1.060	0.562	0.378

TABLE 1. Variation of three-dimensional pressure drop and flow distribution in the toroidal duct with d

flux carried by layer F increases and that carried by layer ST decreases because, owing to the shorter distance between the two walls more isolines of the bottom potential enter the vicinity of wall 1. Thus, decreasing d is associated with more benefits than losses: the increase in the flow rate carried by layer F is higher than the increase in the pressure drop.

In discussing the variation of flow parameters with the toroidal duct length l we start with the 180° bend, when $l = a$, the smallest of possible values. To be consistent with flow for $l > a$, radial ducts 1 and 2 are assumed to be connected only at $x = 0$ so that there is no electrical contact between the radial ducts in the region $x < 0$. The other case, in which wall 6 is common to both radial ducts, can be treated by setting $\phi_6 = 0$ (virtually perfectly conducting wall), since wall 6 would lie in the symmetry plane $y = l = a$. Note that the flow structure in the latter case would be completely different.

In a 180° bend the resistance to the three-dimensional current is lowest. Current which flows in the sidewalls can easily cross the plane $y = l$, choosing the long path. Therefore, the three-dimensional pressure drop is the highest. When l increases, the resistance of the long circuit increases as well and the three-dimensional pressure drop decreases (figure 10).

When $l \rightarrow \infty$, the three-dimensional pressure drop tends towards a finite limit equal to that in a 90° bend. At this limit the y-component of core current in the toroidal duct vanishes (equation ($9g$)), and the core CT becomes current-free. There is no diffusion
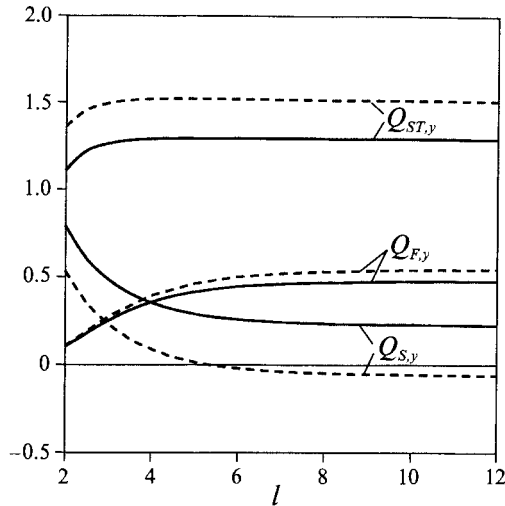
FIGURE 11. Variation of volume fluxes carried by layers F, ST, and S at $y = l$ in the y-direction with l for $c = 0.2$ (———) and $c = 0.1$ (– – –). The total volume flux is 2.

of the bottom potential through the core. The bottom potential becomes higher, pumping in the core becomes more intensive, volume fluxes carried by layers F and ST increase, and the volume flux carried by layer S decreases (figure 11). In a 90° bend the flow in the toroidal duct develops very slowly with y. The outer borders of the layers F, ST and S are parabolic in shape. They merge at distances of the order of M, forming a 'wake'. The flow structure is qualitatively similar to that around a body of revolution in a strong uniform magnetic field aligned with the free-stream velocity (see Chang 1963). At distances $O(M)$ the y-component of velocity becomes of order 1. There is no distinct core and layers. When y increases further, the flow slowly tends towards conventional hydrodynamic flow at infinity, so that the development length in the toroidal duct is $O(M)$. Thus, the flow needs a very long distance to attain a fully developed Poiseuille profile. It follows from $(9a, c, e)$ that in a 90° bend the core potential and the x- and z-components of core velocity become functions of x and z only. The total amount of fluid that enters layer F from the core CT, integrated from the bottom of the toroidal duct, grows with y (equation (18)). The amount of fluid that leaves layer F to the layer ST also grows with y to infinity (equation (16)). The difference between the two flow rates tends to become a constant as $y \to \infty$. This constant is equal to the volume flux carried by layer F in the y-direction. The same conclusion applies to the mass exchange between layers ST and S. Thus, all the fluid, except that in the plane $z = 0$, sooner or later becomes involved in a helical motion.

Figure 11 shows another interesting feature of the flow. For $c = 0.2$, the flow structure in the toroidal duct for $l \geqslant 2$ is qualitatively the same as in the reference case. There are only quantitative changes in flow distribution between the layers.

For lower values of the wall conductance ratio, at a certain value of $l = l_*$ the flow in layer S may become reversed. For $c = 0.1$, this happens at $l_* = 5.41$. The flow distribution in the toroidal duct for $c = 0.1$ and $l = 12$ is shown in figure 8. For $l > l_*$, close to the symmetry plane $y = l$, there is a high-velocity jet in layer S in the $-y$-direction, as a result of a strong pumping in the core. In layer S there is a surface on which the y-component of velocity vanishes so that the flow must enter the core. Streamlines are shown in figure 12. Long streamlines are qualitatively the same as those
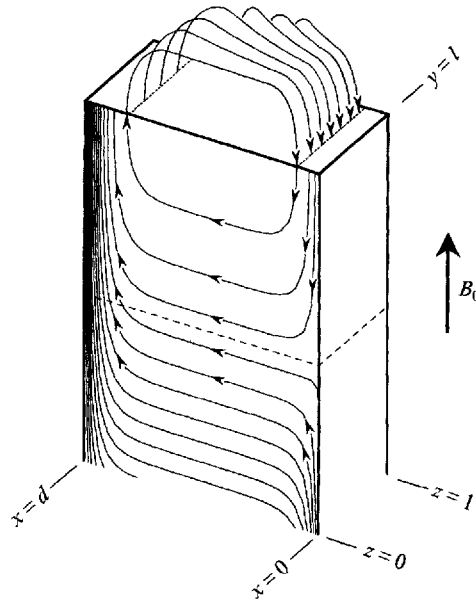
FIGURE 12. Sketch of streamlines close to the plane $y = l$ for $l > l_*$, showing vortex structure.

described above in the reference case. The second type of streamline is associated with the vortex, which exists near the plane of symmetry $y = l$. When the fluid crosses the symmetry plane $y = l$ in the $-y$-direction in the layer S, it first flows downward, and then leaves the layer towards the core CT. Having passed the core and entered layer F or ST, the fluid crosses the symmetry plane $y = l$ within these layers. Then it must return to layer S in the part $y > l$ of the toroidal duct in a symmetric way. Only parts of layers F and ST close to the core are involved in a vortex motion. The other parts closer to the walls carry all the volume flux in the y-direction so that the rest of the fluid flows around the vortex. The vorticity in the core

$$\omega_{CT} = \frac{1}{l}\frac{\partial \phi_4}{\partial x}\hat{x} + \left(1 - \frac{y}{l}\right)\frac{1}{c_4}j_{yCT}\hat{y} + \frac{1}{l}\frac{\partial \phi_4}{\partial z}\hat{z}$$

is of order 1 and is essentially not aligned with the magnetic field. The common view (Sommeria & Moreau 1982; Sommeria 1988) is that vortices with such a property are strongly damped by a magnetic field. In contrast, the vortex considered here is created by a strong MHD interaction. Obviously, the U-bend geometry promotes such a flow pattern.

Consider now the variation of flow parameters with the wall conductance ratio. For $c = 0.2$ most of the volume flux is carried by layer ST. Layer F carries 24.1% of the total volume flux. When c increases, the absolute value of the induced potential decreases, so that the potentials of walls 1, 3, 4 become lower. As a result, the volume fluxes carried by layers F and ST decrease and that carried by layer S increases (figure 13). If $c \gg 1$, all the volume flux is confined to a jet at wall 2 so that a Hunt-type flow occurs. The potentials of all walls of the toroidal duct tend towards zero, and the core CT becomes stagnant.

If c decreases, the volume flux carried by layer S decreases, and if $c = 0.106$, the flow at wall 2 at the symmetry plane $y = l$ becomes reversed. The streamlines are qualitatively the same as those in figure 12. If $c \ll 1$, the total flow is confined to the jets at the sidewalls. However, if c decreases from 0.106, the reversed flow in layer S
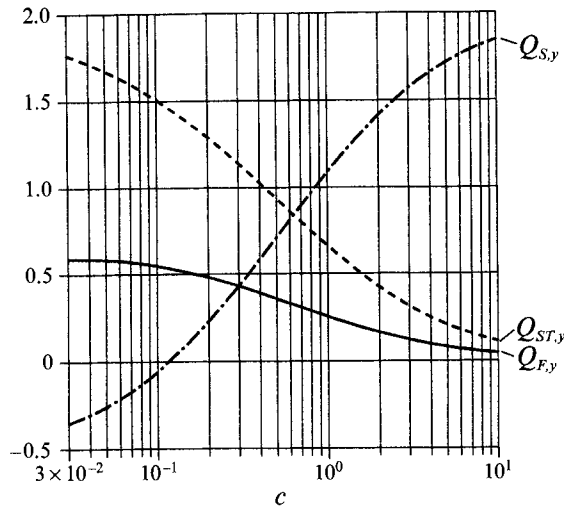
FIGURE 13. Variation of volume fluxes $Q_{F,y}$ (——), $Q_{ST,y}$ (---) and $Q_{S,y}$ (—·—·—) at $y = l$ with c. The total volume flux is 2.
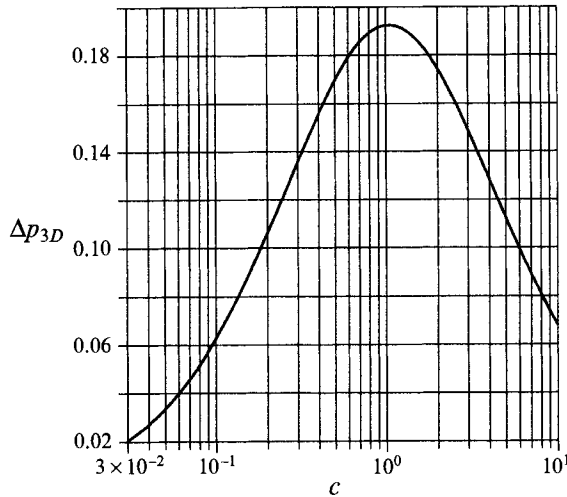
FIGURE 14. Variation of Δp_{3D} with c.

first becomes more intensive, and only from the value of $c = 0.005$ does it start to decrease. This means that Hunt & Holroyd's prediction is valid for very low values of the wall conductance ratio.

In both extreme cases of very high and very low values of c, the core CT is stagnant, the jet in layer F vanishes, and the first wall is uncooled.

Figure 14 shows that the three-dimensional pressure drop reaches a maximum roughly at $c = 1$. When $c \to 0$, the magnitude of the three-dimensional current becomes small; when $c \gg 1$, the walls of the ducts become very good conductors so that the potential difference between the sidewalls of the radial duct tends towards zero. In both cases $\Delta p_{3D} \to 0$.

We now relax the assumption of equal wall conductance ratio of all walls. This gives a wide variety of flow patterns. If wall 1 is perfectly conducting, i.e. $c_1 = \infty$, then $\phi_1 = 0$. Lines of constant bottom potential do not enter wall 1, but wall 3. A jet in layer
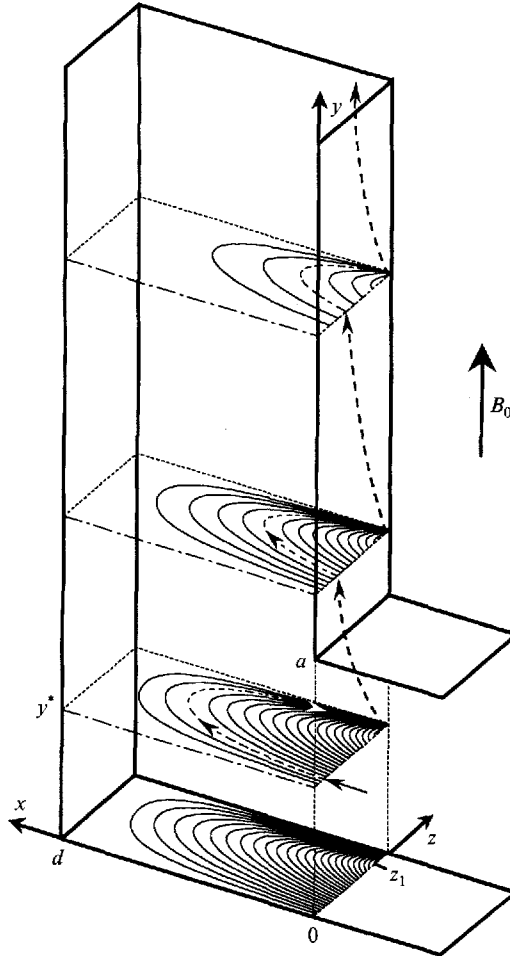
FIGURE 15. Isolines of bottom potential ϕ_4 and sketch of streamlines in the toroidal duct with perfectly conducting walls 1 and 3.

F vanishes, and only the core CT, and layers I, S and ST are involved in a helical motion. Most of the volume flux is carried by the jet at wall 2. If both walls 1 and 3 are perfectly conducting ($c_1 = c_3 = \infty$), both the potentials ϕ_1 and ϕ_3 are zero. The jets at walls 1 and 3 vanish, and the total volume flux is carried by layer S. Only the core CT and layers S and I are involved in a helical motion. Isolines of bottom potential leave the junction, and return after making a turn of about 180° (figure 15). Thus, the fluid in the part $0 < z < z_1$ close to the plane of symmetry $z = 0$ enters, for example, layer I from the core CR of the radial duct, leaves it at a cross-section $y = y^*$ to the core, makes a turn of about 180° in the core CT, and enters layer I again, closer to wall 3 ($z > z_1$) at the same cross-section $y = y^*$ (figure 15). The same holds for layer S. Because there is a volume flux through the core, from the centre of layer S to the region in layer S closer to wall 3, the y-component of velocity in layer S at the centre $z = 0$ is smaller than at corner $A2$. When the fluid enters layer I or S after the cycle, it is redistributed there so that the velocity peak close to wall 3 does not reach infinite values. As in the previous cases, streamlines in this layer are inclined towards the plane of symmetry $z = 0$.

Perhaps the most exotic flow occurs when wall 3 is perfectly conducting, but wall 1
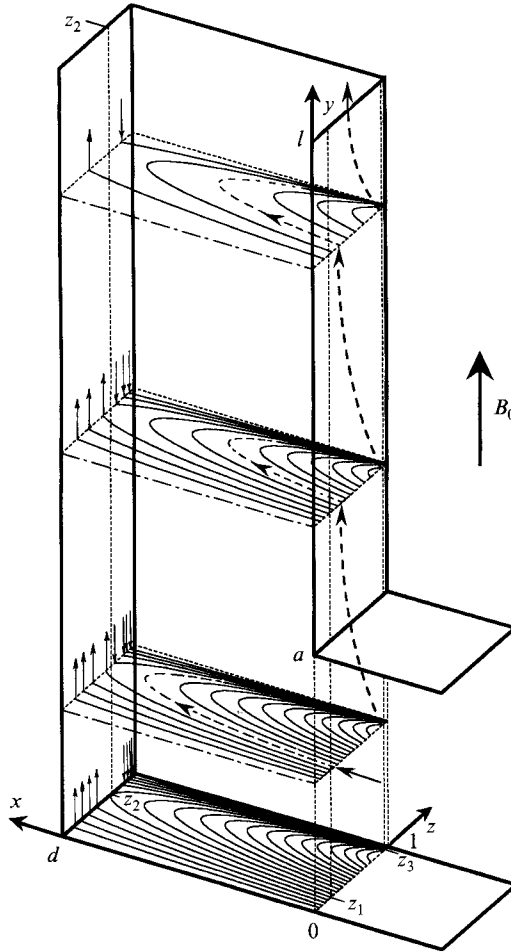
FIGURE 16. Isolines of bottom potential ϕ_4 and sketch of streamlines in the toroidal duct with perfectly conducting wall 3. The flow entering the core CT at $x = 0$, $0 < z < z_1$ enters layer F and flows upward in the region $0 < z < z_2$. The flow entering the core CT at $x = 0$, $z_1 < z < z_3$ bypasses the layer F. The flow at $x = 0$, $z_3 < z < 1$ is taken from layer F in the region $z_2 < z < 1$.

is not ($c_3 = \infty$; $\phi_3 = 0$). The volume flux carried by layer ST is zero, and the total volume flux is carried by layer S. All isolines of the bottom potential enter wall 1 (figure 16), and all the fluid from the core CT is directed towards wall 1. However, the total volume flux carried by layer F is zero (expression (17) with $\phi_1(y, z = 1) = 0$). This means that in layer F the flow is in the y-direction in the region $0 < z < z_2$ ($q_{F,y} > 0$), and in the $-y$-direction closer to wall 3 in the region $z_2 < z < 1$ ($q_{F,y} < 0$). Near wall 3 the flow is reversed not only in layer F, but also in the core, where the fluid flows in the $-x$-direction to join the jet at wall 2.

Finally, if the bottom 4 is either a perfect or a poor conductor, the fluid in the core CT and in layer F is stagnant. The total volume flux is carried by jets at walls 2 and 3 with no helical structures.

4.3. *Comparison with an experiment*

The results obtained with the present theory for a 90° bend were compared with detailed experimental measurements of the wall potential and pressure drop (Barleon *et al.* 1993*b*). The measurements were made in a ⌐-shaped geometry. The two

'toroidal' ducts were connected by a 'radial' duct so that the geometry approximated two 90° bends. The Hartmann number in the experiment varied in the range of 1937–8027, while the interaction parameter varied in the range of 1995–27340 and 10^2–10^5 for potential and pressure measurements, respectively. Theoretical and experimental results for both the pressure and potential are in very good agreement (within the experimental accuracy) for $N > 2000$ and all values of M. The only noticeable disagreement (about 10 %) was found close to the outer corner $x = d$, $y = 0$. The disagreement was probably caused by a recirculatory flow at the corner due to separation effects at moderate values of N. Indirect support for this statement can be found in numerical calculations of flow in a 45° backward elbow performed by Kunugi *et al.* (1991), who observed a vortex at the outer corner.

Such good agreement between the present theory and the experiment is somewhat surprising, since

(i) the experimental measurements were not made in a 90° bend, but in a ⎿-bend. The total length of the 'radial' duct was less than 6, and pressure measurements in the middle of the 'radial' duct indicate that the conditions of fully developed flow were not exactly attained there;

(ii) the value of $c = 0.052$ was not high enough to satisfy the condition $c \gg M^{-\frac{1}{2}}$; in fact, c was of the order of $M^{-\frac{1}{2}}$. In this case, the side layers may conduct non-negligible electric currents, which in turn may affect both the pressure drop and the wall potential;

(iii) the inertialess assumption $N \gg M^{\frac{3}{2}}$ was not realized for all combinations of N and M of the range covered. For $N < 2000$ inertial effects become important. Further work is needed to take into account inertial terms, expecially in the parabolic layers, where high-velocity jets occur.

5. Conclusions

In contrast to the previous notion, the flows in a U-bend and in a 90°-bend for $\alpha = 0°$ exhibit a variety of qualitatively different flow patterns. The flow is very sensitive to the variation of parameters, such as the wall conductance ratio and the distance d between walls 1 and 2. If the wall conductance ratio tends either to zero or to infinity, the volume flux in the toroidal duct is carried by two jets at the sidewalls and by a single jet at wall 2, respectively. In both limiting cases, the core of the toroidal duct is stagnant. However, these flow patterns are realized either for very low or for very high values of the wall conductance ratio which are not relevant to the blanket conditions. If c varies over a wide range, excluding the limiting cases, the volume flux is carried by jets at all duct walls including the first wall. The core does not carry a volume flux in the y-direction. The other two components of core velocity are responsible for the flow distribution between the layers. The volume flux carried by the jet at wall 1 is determined mainly by the pumping effect in the core. In the reference case the jet at wall 1 carries a significant part of the total volume flux. Unlike Moon *et al.* (1991) we find an increasing volume flux carried by the internal layer I and then by layer S with increasing wall conductance ratio.

One of the most surprising results is the presence of the helical and vortex types of flow structures. The helical flow is caused by the exchange of mass between the parabolic layers through the duct corners. At the corners one-dimensional parabolic layers intersect, and two-dimensional parabolic layers are formed. The latter do not affect the flow in the one-dimensional parabolic layers. However, they allow the exchange of mass between one-dimensional layers by high-velocity jets.

The vortex flow is determined mainly by pumping in the core of the toroidal duct. The fluid is taken from the layer at wall 2 in the entire toroidal duct. The volume flux carried by layer S decreases with increasing y, and at a certain distance from the bottom the flow may become reversed. Even more exotic flow patterns may occur if some of the duct walls are perfectly conducting.

The flow in the U-bend is easy to control. The two criteria lead to desirable heat-transfer conditions, namely the high flow rate carried by layer F and the exchange of mass between layers F and ST. The most obvious way to improve heat-transfer conditions is to reduce the distance between walls 1 and 2. This increases not only the average velocity in the toroidal duct due to reduction of the cross-section, but also the percentage of flow rate carried by layer F due to the higher amount of current closing through the first wall. For example, in the radial–toroidal–radial concept of the blanket $d = 0.36$ so that more than half of the flow is carried by the jet at the first wall. This leads to desirable heat-transfer conditions.

REFERENCES

AITOV, T. N., KALYUTIK, A. I. & TANANAEV, A. V. 1979 Numerical investigation of three-dimensional MHD flow in a curved channel of rectangular cross section. *Magnetohydrodynamics* **4**, 458–462.

BARLEON, L., BÜHLER, L., MACK, K. J., MOLOKOV, S., STIEGLITZ, R. *et al.* 1993*a* Investigations of liquid metal flow through a right angle bend under fusion relevant conditions. *Proc. 17th Symp. on Fusion Technology, Rome, Italy, 14–18 September, 1992*, pp. 1276–1280.

BARLEON, L., BÜHLER, L., MACK, K. J., STIEGLITZ, R., PICOLOGLOU, B. F. *et al.* 1992 Liquid metal flow through a right angle bend in a strong magnetic field. *Fusion Technol.* **21**, 2197–2202.

BARLEON, L., BÜHLER, L., MOLOKOV, S. & STIEGLITZ, R. 1993*b* Magnetohydrodynamic flow through a right angle bend. *Seventh Beer-Sheva Intl Seminar on MHD Flows and Turbulence, Israel, February 14–18, 1993* (to be published).

BÜHLER, L. 1993 Magnetohydrodynamische Strömungen flüssiger Metalle in allgemeinen dreidimensionalen Geometrien unter der Einwirkung starker, lokal variabler Magnetfelder. *Kernforschungszentrum Karlsruhe, Rep.* KfK 5095.

CHANG, I. D. 1963 On a singular perturbation problem in magnetohydrodynamics. *Z. Angew Math. Phys.* **14**, 134–147.

COOK, L. P., LUDFORD, G. S. S. & WALKER, J. S. 1972 Corner regions in the asymptotic solution of $\epsilon \nabla^2 u = \partial u / \partial y$ with reference to MHD duct flow. *Proc. Camb. Phil. Soc.* **72**, 117–121.

HOLROYD, R. J. 1980 An experimental study of the effects of wall conductivity, non-uniform magnetic fields and variable area ducts on liquid metal flows at high Hartmann numbers. Part 2. Ducts with conducting walls. *J. Fluid Mech.* **96**, 355–374.

HUA, T. Q. & WALKER, J. S. 1991 MHD considerations for poloidal-toroidal coolant ducts of self-cooled blankets. *Fusion Technol.* **19**, 951–960.

HUA, T. Q., WALKER, J. S., PICOLOGLOU, B. F. & REED, C. B. 1988 Three-dimensional magnetohydrodynamic flows in rectangular ducts of liquid-metal-cooled blankets. *Fusion Technol.* **14**, 1389–1398.

HUNT, J. C. R. & HOLROYD, R. J. 1977 Applications of laboratory and theoretical MHD duct flow studies in fusion reactor technology. *Culham Laboratory Rep.* CLM-R169.

HUNT, J. C. R. & LEIBOVICH, S. 1967 Magnetohydrodynamic flows in channels of variable cross-section with strong transverse magnetic field. *J. Fluid Mech.* **28**, 241–260.

KUNUGI, T., TILLACK, M. S. & ABDOU, M. A. 1991 Analysis of liquid metal MHD fluid flow and heat transfer using the KAT code. *Fusion Technol.* **19**, 1000–1005.

MALANG, S., *et al.* 1988 Self-cooled liquid-metal blanket concept. *Fusion Technol.* **14**, 1343–1356.

MOLOKOV, S. & BÜHLER, L. 1993 Numerical simulation of liquid-metal flows in radial-toroidal-radial bends. *Kernforschungszentrum Karlsruhe, Rep.* KfK 5160.

MOON, T. J., HUA, T. Q. & WALKER, J. S. 1991 Liquid metal flow in a backward elbow in the plane of a strong magnetic field. *J. Fluid Mech.* **227**, 273–292.

MOON, T. J. & WALKER, J. S. 1990 Liquid metal flow through a sharp elbow in the plane of a strong magnetic field. *J. Fluid Mech.* **213**, 397–418.

SMITH, D. L. *et al.* 1985 Blanket comparison and selection study. *Fusion Technol.* **8**, 1.

SOMMERIA, J. 1988 Electrically driven vortices in a strong magnetic field. *J. Fluid Mech.* **189**, 553–569.

SOMMERIA, J. & MOREAU, R. 1982 Why, how, and when, MHD turbulence becomes two-dimensional. *J. Fluid Mech.* **118**, 507–518.

TILLACK, M. S. & McCARTHY, K. A. 1989 Flow quantity in side layers for MHD flow in conducting rectangular ducts. *University of California, Los Angeles, Rep.* UCLA-IFNT-89-01.

WALKER, J. S. 1981 Magnetohydrodynamic flows in rectangular ducts with thin conducting walls. *J. Méc.* **20**, 79–112.